Journal of
Ceramic Science
and Technology

*J. Ceram. Sci. Tech.*, 07 [04] 329-334 (2016)
DOI: 10.4416/JCST2016-00028
available online at: http://www.ceramic-science.com


# Structural, Electrical and Magnetic Properties of $BiFe_{1-x}Y_xO_3$ ($0 \le x \le 0.6$) Ceramics

**A.A.A. Najm, A.H. Shaari*, H. Baqiah, E. Bin Saion, L.K. Pah, C.S. Kien and M.M.A. Kechik**

Department of Physics, Faculty of Science, Universiti Putra Malaysia, 43400 Serdang, Selangor, Malaysia
received March 28, 2016; received in revised form May 22, 2016; accepted June 1, 2016

**Abstract**

**The effect of Y substitution on the microstructure, dielectric, magnetic and leakage current properties of $BiFe_{1-x}Y_xO_3$ ($0 \le x \le 0.6$) ceramics was investigated. The $BiFeO_3$ phase that is dominant at $x = 0.0 - 0.2$ decreased with the increase of Y substitution. Other phases such as $YFeO_3$ and $Bi_{1.46}Y_{0.54}O_3$ emerged with Y substitution and became dominant in the range $x = 0.3 - 0.4$ and $0.5 - 0.6$, respectively. The $BiFe_{1-x}Y_xO_3$ composites of rounded shape grains at $x = 0.0$ deformed at $x = 0.1 - 0.3$ and changed to melted-like grains at $x = 0.4 - 0.6$ with the incorporation of smaller grains at $x = 0.5$ and 0.6. The sample with $x = 0.2$ had the highest remnant magnetization ($Mr = 0.09$ emu/g) and saturation magnetization ($Ms = 2.9$ emu/g). The sample with $x = 0.4$ showed the highest dielectric constant of 104 and lowest loss tangent of $1.34 \times 10^{-4}$. The leakage current was significantly reduced to a lower value of $2.80 \times 10^{-8}$ A/cm$^2$ at $x = 0.6$.**

*Keywords: Bismuth ferrite ceramic, x-ray diffraction, solid-state reaction, magnetic properties, dielectric properties*

## I. Introduction

Multiferroics are compounds that demonstrate the presence of two or three orderings of ferromagnetic, ferroelectric as well as ferroelastic properties. Increasing interest in these materials is derived from their vital applications such as in memory components, reverberation gadgets and transducers [1–4]. The magnetoelectric coupling (ME), that is mean control of the electric polarization with a magnetic field and vice versa, is an important characteristic of multiferroics for data storage applications [5–7].

Taking a glance at the numerous advances in this field, distorted perovskite ($ABO_3$) structured of $BiFeO_3$ (BFO) is an intriguing multiferroic material with regard to its high antiferromagnetic Neel temperature ($T_N \sim 643$ K) as well as its ferroelectric transition, Curie temperature (Tc ~ 1103 K) over room temperature [8]. However, BFeO ceramic has some limitations such as high leakage current density [5] and weak magnetic behavior that restrict its application [9]. On the other hand, preparation of single-phase BFO involves some difficulties owing to narrow temperature level of phase stabilization [10]. Several secondary phases have been stated in early reports, mainly comprising $Bi_2Fe_4O_9$, $Bi_{12}(Bi_{0.5}Fe_{0.5})O_{19.5}$ and $Bi_{25}FeO_{40}$ [11].

Chemical replacement is an active tool to control multiferroic properties of BFeO [12]. For example, doping with alkali earth atoms like (Ca, Sr, Ba, etc.) in Bi-sites of the BFO has shown enhancement of its magnetic and ferroelectric properties. Recent papers suggested that the maximum magnetization occurrence and leftover magnetization were prominently utilized for the sample doped with $Ba^{2+}$ at Bi-site [13–18]. The rare earth dopants have been shown to improve both the magnetic and dielectric properties [19]. It has been reported that some rare earth ions doped at the Bi site have reduced leakage current and Curie temperature and enhanced dielectric ordering and structural stability, etc. [20–26]. As an example, doping with Y in Bi sites resulted in increasing magnetization of $Bi_{1-x}Y_xFeO_3$ ceramics [27, 28]. However, few studies concern the incorporation of rare earths in the Fe site of BFO. The Y is one of rare earths that has the same valence as $Fe^{3+}$, while the ionic radius of $Y^{3+}$ (1.019 Å) is greater than that of $Fe^{3+}$ (0.78 Å). Detailed studies of the interplay between the structural, dielectric and magnetic properties in Y-substituted Fe sites of the single-phase BFO system are highly desirable with regard to possible applications. Hence, we aimed to produce $BiFe_{1-x}Y_xO_3$ ceramics ($0 \le x \le 0.6$) according to the conventional solid-state route. The effect of $Y^{3+}$ substitution on the structure, leakage current, dielectric and magnetic properties of $BiFe_{1-x}Y_xO_3$ ($0 \le x \le 0.6$)system is reported.

## II. Experimental Procedure

The $BiFe_{1-x}Y_xO_3$ ($x = 0.0 - 0.6$) solid solution was prepared according to the conventional solid state route. A stoichiometric amount of high-purity $Bi_2O_3$ (99.9 %), $Fe_2O_3$ (99.98 %) and $Y_2O_3$ (99.99 %) were weighed, ground and homogenized with a pestle and mortar. The powder was calcined for 2 h at a temperature of 780 °C and further ground for an additional 1 h, which resulted in a homogeneous fine powder. The powder was pelletized to a size of 13 mm diameter and ~2 mm thickness using

* Corresponding author: ahalim@upm.edu.my

polyvinyl alcohol (0.05 mL $g^{-1}$) as a binder with the application of 5 t pressure. The pellets were then sintered in air for 3 h at 800 °C. The crystal structure of the samples was studied by means of X-ray diffraction (XRD) using a Philips X'Pert diffractometer model 7602 EA Almelo with Cu Kα radiation source with λ = 1.5418 Å. The diffraction pattern was recorded at room temperature with 2θ scanning range from 20° to 80°. Structural morphology and chemical composition of the samples were studied using scanning electron microscope (SEM) (SEM, JEOL JSM-6400) incorporating with Energy Dispersive X-ray (EDX). The magnetic properties of the pure and doped samples were studied using a vibrating sample magnetometer (VSM) (Lakeshore model 7407 VSM). The dielectric constant and loss factor of the samples were measured at room temperature using an impedance analyzer (Agilent 4294A precision impedance analyzer) at a frequency range of 40 Hz – 10 MHz at room temperature. The leakage current of samples was evaluated using a sourcemeter unit (2400 Sourcemeter, Keithley Instruments Inc.). The two sides of the sintered pellets were polished and coated with silver paste to create electrodes for dielectric and current leakage measurement.

## III. Results and Discussion

### *(1) Structural analysis*

The XRD patterns of $BiFe_{1-x}Y_xO_3$ ($0.0 \le x \le 0.6$) are shown in Fig. 1. The crystal structure, phases and lattice parameters of the samples were analyzed with the Rietveld refinement method using *X'Pert High Score Plus* software and listed in Table 1 and Table 2. The XRD results indicate that unsubstituted $BiFeO_3$ has been formed in single phase with hexagonal structure, space group *R3c* without any secondary phases. Previously, the difficulty of preparing a single phase of $BiFeO_3$ with the conventional solid-state synthesis procedure has been described [8]. The secondary phase such as $Bi_2Fe_4O_9$ and $Bi_{25}FeO_{40}$ was seen at high temperatures such as 850 and 870 °C [29]. It is believed that sintering at low temperature, 800 °C, helped to stabilize $BiFeO_3$ phase owing to the volatile behavior of $Bi_2O_3$ at high temperature [30]. The $BiFeO_3$ phase decreases with Y substitution, but it is still dominant in samples with $x = 0.1$ and 0.2. In addition, it was found that the lattice constant and volume of the unit cell of $BiFeO_3$ phase decreased with increasing concentration of $Y^{3+}$ substitution. This indicates that Y, ion radius (1.019 Å), may have occupied $Bi^{3+}$ site, ion radius (1.17 Å), which leads to the decrease in the lattice constant [31].

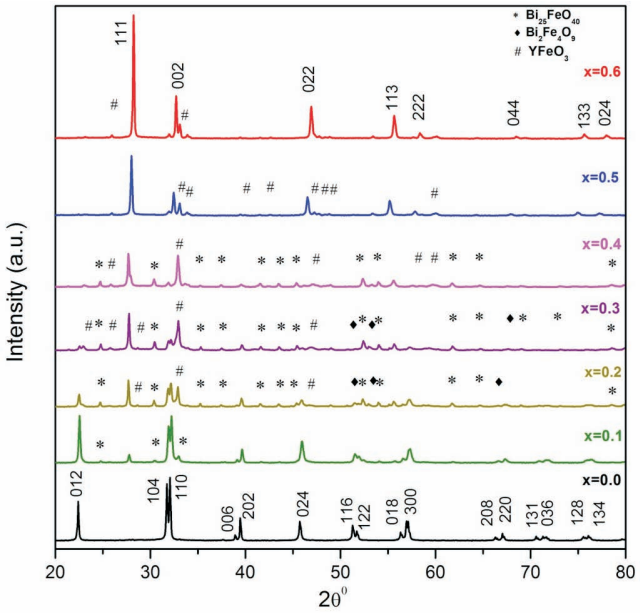


**Fig. 1:** XRD spectra of $BiFe_{x-1}Y_xO_3$ ($x = 0.0 - 0.6$) samples.

**Table 1:** Space group, lattice parameters, crystal system, unit cell volume (V) and good of fitness of $BiFe_{1-x}Y_xO_3$.

| *x* | Phases & percentage (%) | Space group | a (Å) | b(Å) | c (Å) | a/c | Crystal system | V(Å$^3$) | Good of fitness |
|---|---|---|---|---|---|---|---|---|---|
| 0.0 | $BiFeO_3$ 100% | R3c 161 | 5.5784 ±0.0002 | 5.5784 ±0.0002 | 13.8680 ±0.0006 | 0.4022 | Hexagonal | 373.724 | 5.32 |
| 0.1 | $BiFeO_3$ 85.8% | R3c 161 | 5.5680 ±0.0004 | 5.568 ±0.0004 | 13.8340 ±0.0001 | 0.402 | Hexagonal | 371.419 | 5.505 |
| 0.2 | $BiFeO_3$ 35.6% | R3c 161 | 5.5657 ±0.0004 | 5.5657 ±0.0004 | 13.8190 ±0.0010 | 0.4027 | Hexagonal | 370.709 | 4.07 |
| 0.3 | $YFeO_3$ 49.7% | P n m a 62 | 5.6269 ±0.0022 | 7.7243 ±0.0024 | 5.3628 ±0.0017 | 1.0492 | Orthorhombic | 233.094 | 3.81 |
| 0.4 | $YFeO_3$ 48.9% | P n m a 62 | 5.6139 ±0.0013 | 7.6683 ±0.0015 | 5.3234 ±0.0010 | 1.0545 | Orthorhombic | 229.17 | 3.227 |
| 0.5 | $Bi_{1.46}Y_{0.54}O_3$ 56.1% | Fm-3m 225 | 5.5212 ±0.0003 | 5.5212 ±0.0003 | 5.5212 ±0.0003 | 1 | Cubic | 168.306 | 4.608 |
| 0.6 | $Bi_{1.46}Y_{0.54}O_3$ 83.4% | Fm-3m 225 | 5.4766 ±0.0002 | 5.4766 ±0.0002 | 5.4766 ±0.0002 | 1 | Cubic | 164.2604 | 4.603 |

**Table 2:** The percentage of $BiFe_{1-x}Y_xO_3$ phases and ICSD reference code ($x = 0.0 - 0.6$).

| Samples ($x$) / Percentage of phases (%) | 0.0 | 0.1 | 0.2 | 0.3 | 0.4 | 0.5 | 0.6 | References code ICSD |
|---|---|---|---|---|---|---|---|---|
| $BiFeO_3$ | 100 | 85 | 35.60 | 11.50 | 0.90 | 0.00 | 0.00 | 980066143 |
| $Bi_{25}FeO_{40}$ | 0.00 | 13.40 | 25.90 | 25.70 | 36.20 | 0.00 | 0.00 | 980022156 |
| $Bi_2Fe_4O_9$ | 0.00 | 0.00 | 1.20 | 1.0 | 0.00 | 0.00 | 0.00 | 980009807 |
| $Bi_{1.46}Y_{0.54}O_3$ | 0.00 | 0.80 | 3.90 | 12.10 | 14.0 | 56 | 83.40 | 980024637/980021230 |
| $YFeO_3$ | 0.00 | 0.00 | 33.40 | 49.70 | 48.90 | 44 | 16.60 | 980048662 |

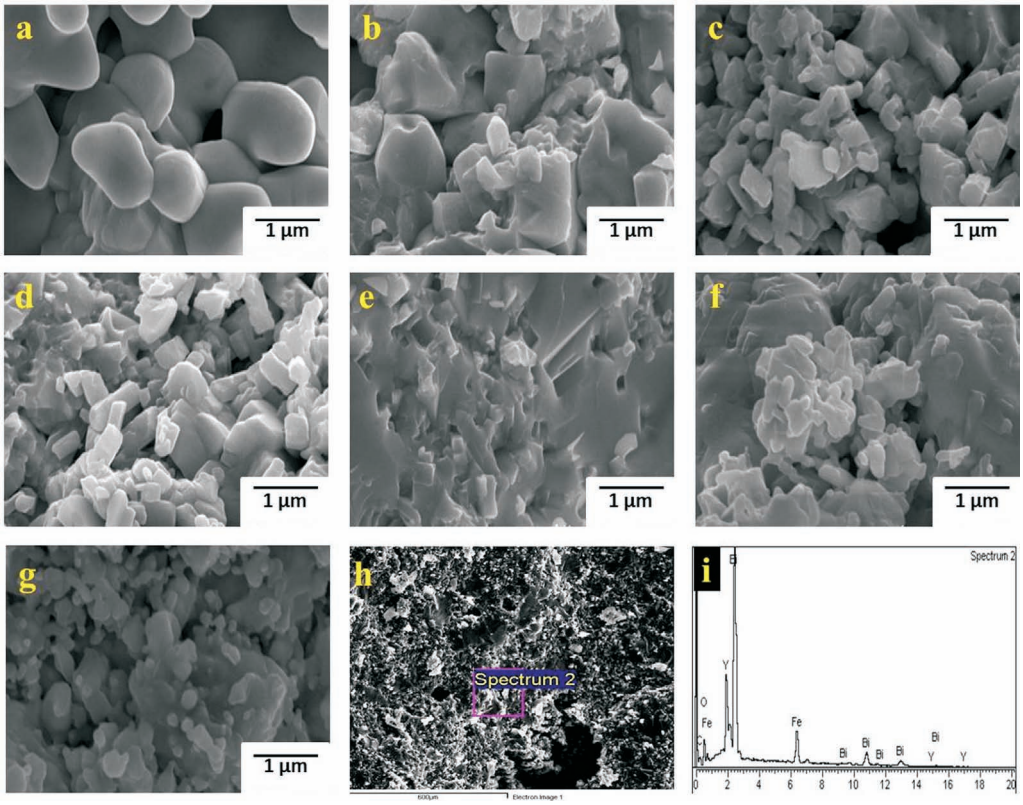


**Fig. 2:** SEM photographs of $BiFe_{1-x}Y_xO_3$ ceramics with (**a**) $x = 0.0$, (**b**) $x = 0.1$, (**c**) $x = 0.2$, (**d**) $x = 0.3$, (**e**) $x = 0.4$, (**f**) $x = 0.5$, (**g**) $x = 0.6$. Fig. (**i**) shows an EDX pattern recorded from image (**e**).

Again from Fig. 1, the peaks of $BiFeO_3$ decreased with increase of Y substitution, and new peaks representing new compounds such as $Bi_2Fe_4O_9$, $Bi_{25}FeO_{40}$, $Bi_{1.46}Y_{0.54}O_3$ and $YFeO_3$ were observed with Y substitution. The size of $Y^{3+}$ is larger than $Fe^{3+}$ ion by 15 %, effective radius of $Y^{3+}$ and $Fe^{3+}$ atomsare 1.019 Å and 0.78 Å, respectively [32]. This makes entry of $Y^{3+}$ into the $Fe^{3+}$ site difficult. The phase's percentage at different Y concentrations is listed in Table 2. The major phase of $BiFeO_3$ started to decrease at $x = 0.1$ and it completely disappeared at $x = 0.5$. On the other hand, other phases such as $YFeO_3$ and $Bi_{1.46}Y_{0.54}O_3$ that emerged with Y substitution become dominant in the range $x = 0.3 - 0.4$ and $0.5 - 0.6$, respectively.

### *(2) Microstructural analysis*

The morphological structure of all the samples examined with SEM are presented in Fig. 2. The SEM images of $BFe_{1-x}Y_xO_3$ ($x$ = 0.0, 0.1, 0.2, 0.3, 0.4, 0.5 and 0.6) revealed that the samples' density and grain morphology are clearly affected by Y substitution. The grains were found to be adhered and agglomerated to each other in different masses. The grain with roundish edge was observed at $x = 0.0$ whereas their shape was deformed at $x = 0.1$. The grain size of $x = 0.2$ and 0.3 was reduced while their shape was almost close to that of the sample with $x = 1$. The calculated grain sizes are displayed in Table 3. As the concentrations of $Y^{3+}$ increased, i.e. $x < 0.3$, a compact, melted-like surface with small particles attached was observed, which made assessment of the grain size difficult. The most compact surface was observed for sample with $x = 0.4$.

### *(3) Dielectric properties*

The dielectric constant ($\varepsilon_r$) and dielectric loss ($tan\ \delta$) versus frequency of $BiFe_{1-x}Y_xO_3$ ceramics measured at room

temperature are presented in Figs. 3a and b. The dielectric constant ($\varepsilon_r$) values ranged between (20 to 104) for $BiFe_{1-x}Y_xO_3$ ($x$ = 0.0 – 0.6), at 1 kHz, see Table 3. Moreover for all samples, the $\varepsilon_r$ declined with a step-up in frequency in the range 40 Hz – 10 MHz, which turned out to be linearly constant at $10^5$ Hz. This is mainly attributed to the different types of polarization such as space charge, nuclear, ionic, dipolar and electronic contributions [33]. It is known that a dielectric material has high dielectric constant at low frequencies, where the space charges are able to follow the frequency of the applied field. While at high frequencies, the $\varepsilon_r$ and tan δ became linear owing to the limited time to build up and undergo relaxation [34]. It is believed that the increase in sample density and grain morphology result in an increment of dielectric constants of Y-substituted $BiFe_{1-x}Y_xO_3$ ($x$ = 0.0 – 0.6) [35]. As a result, the highest value for the dielectric constant (104) and low loss tangent $1.34 \times 10^{-4}$ was observed for the sample with $x$ = 0.4, which has the highest density as evident from SEM.

### *(4) Magnetic properties*

The magnetization versus magnetic field of $BiFe_{1-x}Y_xO_3$ ceramics materials was measured at room temperature in a magnetic field up to 10000 Oe as shown in Fig. 4 and its inset. It is observed from the figure inset that the M-H plot of BFO presented linear magnetic field dependence of the magnetization (*Ms*), which demonstrates antiferromagnetic (AFM) behavior. In fact, the low remnant magnetization (*Mr*) exhibited by this material (as shown in Fig. 4) also affirms its AFM nature [36]. The incorporation of $Y^{3+}$ ions into the BFO lattices enhanced the *Mr* and *Ms*. As the $Y^{3+}$ content rises up to $x$ = 0.2, the *Ms* increased to the highest value, 2.9 emu/g. With increasing concentrations of $Y^{3+}$ above $x$ = 0.2, the *Mr* and *Ms* decreased gradually. On the other hand, an unsaturated hysteresis loop was observed for the compositions with $x$ = 0.4 – 0.6 as shown in Fig. 4 and inset. This indicated that the samples have mixed para- and ferromagnetic characteristics. The value of *Ms* and remnant magnetization *Mr* are listed in Table 3. The remnant value (*Mr* = 0.09 emu/g) and saturate magnetization (*Ms* = 2.9 emu/g) for $x$ = 0.2 sample have significantly increased compared to the value for pure $BiFeO_3$ (*Ms* = 0.001 emu/g).

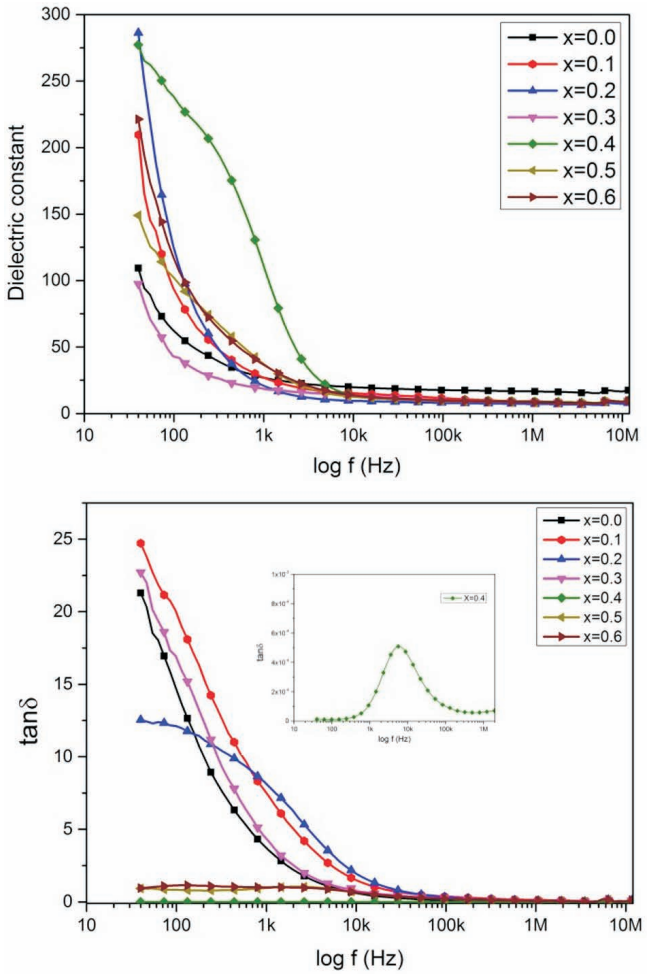


**Fig. 3:** Room temperature dielectric constant (**a**) and loss tangent (**b**) as a function of frequency of $BiFe_{1-x}Y_xO_3$ ($x$ = 0, 0.1, 0.2, 0.3, 0.4, 0.5 and 0.6) samples.

**Table 3:** Grain size, dielectric constant ($\varepsilon_r$), loss tangent, tanδ, Leakage current density an applied electric field of 120.8 V, magnetization (*Ms*) and remnant magnetization (*Mr*) of $BiFe_{1-x}Y_xO_3$($x$ = 0.0 - 0.6) ceramics.

| **Compositions** | Average grain size ($\mu$m) | $\varepsilon_r$ | tanδ | Leakage current density (A/cm$^2$) At applied electric field of 120.8 V·cm$^{-1}$ | *Ms*(emu/g) | $10^{-3}$ *Mr (emu/g)* |
|---|---|---|---|---|---|---|
| $BiFeO_3$ | 2.00±0.10 | 26.53 | 3.52 | $9.24 \times 10^{-4}$ | 0.04 | 2.5 |
| $BiFe_{0.9}Y_{0.1}O_3$ | 2.10±0.20 | 26.21 | 7.23 | $2.83 \times 10^{-4}$ | 0.19 | 6.5 |
| $BiFe_{0.8}Y_{0.2}O_3$ | 0.53±0.03 | 20.02 | 7.93 | $5.66 \times 10^{-5}$ | 2.9 | 90.0 |
| $BiFe_{0.7}Y_{0.3}O_3$ | 0.53±0.05 | 18.26 | 4.13 | $7.34 \times 10^{-4}$ | 1.6 | 47.0 |
| $BiFe_{0.6}Y_{0.4}O_3$ | 0.45±0.05 | 104.4 | $1.34 \times 10^{-4}$ | $1.57 \times 10^{-6}$ | 0.04 | 1.0 |
| $BiFe_{0.5}Y_{0.5}O_3$ | 0.66±0.08 | 35.74 | 0.97 | $5.32 \times 10^{-8}$ | 0.04 | 0.1 |
| $BiFe_{0.4}Y_{0.6}O_3$ | 0.63±0.09 | 35.28 | 1.01 | $2.80 \times 10^{-8}$ | 0.02 | 1.5 |

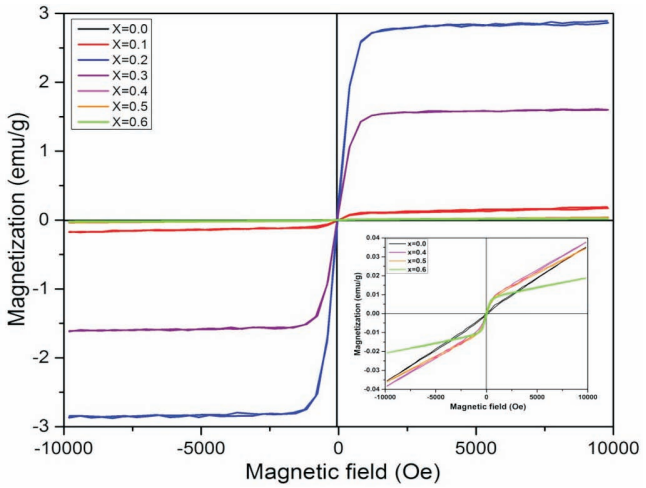


**Fig. 4:** Magnetization hysteresis (M-H) loops of $BiFe_{1-x}Y_xO_3$ ($0.0 \le x \le 0.6$) ceramics measured at room temperature. The inset shows their remnant magnetization (*Mr*).

Since $Y^{3+}$ is a nonmagnetic ion, Y substitution has no direct effect with regard to the enhancement of ferromagnetism. The major source of ferromagnetism is from the interaction of $Fe^{3+}$– $O^{2-}$– $Fe^{3+}$. Yuan *et al.* reported that $Y^{3+}$ doping in $LuFeO_3$ resulted in increased ferromagnetism on the structural modification of $FeO_6$ octahedra [37]. $YFeO_3$ is a canted antiferromagnet with weak saturated magnetization of about (0.18 emu/g) which is less than $BiFe_{0.8}Y_{0.2}O_3$ (2.9 emu/g). Moreover the coercivity of $YFeO_3$ (970 Oe) is far above that of $BFe_{0.8}Y_{0.2}FeO_3$ (20 Oe) [38]. On the other hand, ferromagnetism in $BiFeO_3$ might occur owing to the distortion of cycloidal modulation and the canted antiferromagnetic spin structure [39]. Hence, the magnetic behavior of the samples may be attributed to the distortion of the structure of $BiFeO_3$ and the formation of $YFeO_3$ phase as indicated from XRD result.

### *(5) Leakage current*

The leakage current density versus applied electric field (*J-E*) characteristics curves measured at room temperature of $BiFe_{1-x}Y_xO_3$ ($x$ = 0, 0.1, 0.2, 0.3, 0.4, 0.5 and 0.6) samples are presented in Fig. 5. The leakage current density of Y-substituted samples at an applied electric field of 120.8 $V \cdot cm^{-1}$ were found to be $9.24 \times 10^{-4}$, $2.83 \times 10^{-4}$, $5.66 \times 10^{-5}$, $7.34 \times 10^{-4}$, $1.57 \times 10^{-6}$, $5.32 \times 10^{-8}$ and $2.8 \times 10^{-8}$ $A \cdot cm^{-2}$ for $BiFe_{1-x}Y_xO_3$ ($x$ = 0.0, 0.1, 0.2, 0.3, 0.4, 0.5, and 0.6) ceramics respectively. It is known that high current leakage of BFO is due to the mixed valence of Fe ions ($Fe^{3+}$ and $Fe^{2+}$) generated by the presence of oxygen vacancies, which results in the increase in the conductivity [40]. As $Y^{3+}$ substitution increased, leakage current density significantly decreased to lower values for all concentrations of $BiFe_{1-x}Y_xO_3$ as compared to the values in the pure sample. The leakage currents observed in pure and substituted $BiFeO_3$ ceramics are developed mainly from charge defects, in particular bismuth vacancies ($V_{Bi}^{2+}$) and oxygen vacancies ($V_O^{2+}$) [41]. For the studied samples, it is believed that the change of $BiFeO_3$ unit cell and formation of new phases are the main factors that control the leakage current property of the samples.

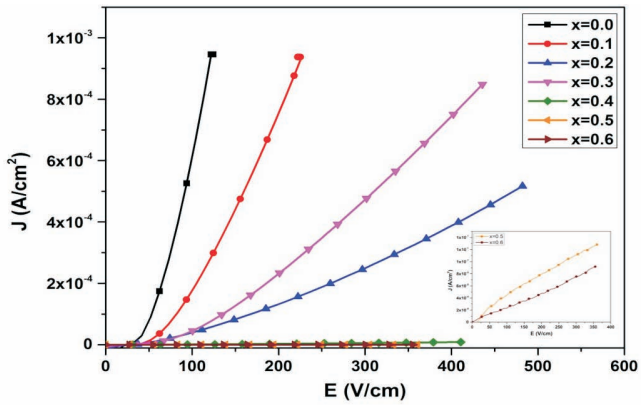


**Fig. 5:** Leakage current density versus applied electric field (J-E) of $BiFe_{1-x}Y_xO_3$ ceramic measured at room temperature.

## IV. Conclusions

The effect of yttrium substitution on the microstructure, magnetic, dielectric and current leakage properties of $BiFe_{1-x}Y_xO_3$ ($x$ = 0.0 – 0.6) ceramics was investigated. From the XRD result, the $BiFeO_3$ phase that is dominant at $x$ = 0.0 – 0.2, decreased with increase of Y substitution. Other phases such as $YFeO_3$ and $Bi_{1.46}Y_{0.54}O_3$ were formed with Y substitution and became dominant in the range of $x$ = 0.3 – 0.4 and 0.5 – 0.6, respectively. The $BiFe_{1-x}Y_xO_3$ samples with x = 0.0 exhibited rounded shape like grains which deformed in the case of the sample with $x$ = 0.1 – 0.3 and changed to melted-like grains at $x$ = 0.4 – 0.6 with the incorporation of small grains at $x$ = 0.5 and 0.6. The highest dielectric constant, $\varepsilon_r$ = 104, and lowest loss tangent, $\tan\delta = 1.34 \times 10^{-4}$, were observed at $x$ = 0.4 as a result of the increase in sample density while the highest magnetization (*Ms*), 2.9 emu/g, for $x$ = 0.2, may be attributed to the distortion of the structure of $BiFeO_3$ and the generation of $YFeO_3$ phase. The leakage current decreased with increasing concentrations of Y substitution. In conclusion, yttrium substitution resulted in a tunable multiferroic order in $BiFe_{1-x}Y_xO_3$ ceramics. The sample with $x$ = 0.4 is probably the best sample, combining good magnetic, dielectric and leakage current properties.

## Acknowledgments

The authors would like to thank Ministry of Education Malaysia (MOE) for supporting this research with grant NO: FRGS5524554.

## References

1 Wang, J., Neaton, J., Zheng, H., Nagarajan, V., Ogale, S., Liu, B., Viehland, D., Vaithyanathan, V., Schlom, D., Waghmare, U.: Epitaxial $BiFeO_3$ multiferroic thin film heterostructures, *Science*, **299**, 1719 – 1722, (2003).

2 Nuraje, N., Dang, X., Qi, J., Allen, M.A., Lei, Y., Belcher, A.M.: Biotemplated synthesis of perovskite nanomaterials for solar energy conversion, *Adv. Mater.*, **24**, 2885 – 2889, (2012).

3 Fiebig, M., Lottermoser, T., Fröhlich, D., Goltsev, A., Pisarev, R.: Observation of coupled magnetic and electric domains, *Nature*, **419**, 818 – 820, (2002).

4 Kanai, T., Ohkoshi, S.i., Nakajima, A., Watanabe, T., Hashimoto, K.: A ferroelectric ferromagnet composed of $(PLZT)_x(BiFeO_3)_{1-x}$ solid solution, *Adv. Mater.*, **13**, 487 – 490, (2001).

5 Bibes, M., Barthélémy, A.: Towards a magnetoelectric memory, *Nat. Mater*, **7**, 425 – 426, (2008).

6 Smolenskiĭ, G., Chupis, I.: Ferroelectromagnets, *Sov. Phys. Uspekhi*, **25**, 475, (1982).

7 Eerenstein, W., Mathur, N., Scott, J.F.: Multiferroic and magnetoelectric materials, *Nature*, **442**, 759 – 765, (2006).

8 Lazenka, V., Zhang, G., Vanacken, J., Makoed, I., Ravinski, A., Moshchalkov, V.: Structural transformation and magnetoelectric behaviour in $Bi_{1-x}Gd_xFeO_3$ multiferroics, *J. Phys. D: Appl. Phys.*, **45**, 125002, (2012).

9 Izyumskaya, N., Alivov, Y., Morkoç, H.: Oxides, oxides, and more Oxides: High-$\varkappa$ oxides, ferroelectrics, ferromagnetics, and multiferroics, *Crit. Rev. Solid State Mater. Sci.*, **34**, 89 – 179, (2009).

10 Muneeswaran, M., Jegatheesan, P., Gopiraman, M., Kim, I.-S., Giridharan, N.: Structural, optical, and multiferroic properties of single phased $BiFeO_3$, *Appl. Phys. A* , **114**, 853 – 859, (2014).

11 Nalwa, K., Garg, A., Upadhyaya, A.: Effect of samarium doping on the properties of solid-state synthesized multiferroic bismuth ferrite, *Mater. Lett.*, **62**, 878 – 881, (2008).

12 Yang, C.-H., Kan, D., Takeuchi, I., Nagarajan, V., Seidel, J.: Doping $BiFeO_3$: approaches and enhanced functionality, *Phys. Chem. Chem. Phys.*, **14**, 15953 – 15962, (2012).

13 Naik, V., Mahendiran, R.: Magnetic and magnetoelectric studies in pure and cation doped, *Solid State Commun.*, **149**, 754 – 758, (2009).

14 Ramachandran, B., Dixit, A., Naik, R., Lawes, G., Rao, M.R.: Weak ferromagnetic ordering in ca doped polycrystalline $BiFeO_3$, *J. Appl. Phys.*, **111**, 023910, (2012).

15 Bhushan, B., Das, D., Priyam, A., Vasanthacharya, N., Kumar, S.: Enhancing the magnetic characteristics of $BiFeO_3$ nanoparticles by Ca, Ba co-doping, *Mater. Chem. Phys.*, **135**, 144 – 149, (2012).

16 Khomchenko, V., Kiselev, D., Vieira, J., Jian, L., Kholkin, A., Lopes, A., Pogorelov, Y., Araujo, J., Maglione, M.: Effect of diamagnetic Ca, Sr, Pb, and Ba substitution on the crystal structure and multiferroic properties of the $BiFeO_3$ perovskite, *J. Appl. Phys.*, 024105 – 6, (2008).

17 Yang, C., Jiang, J.-S., Qian, F.-Z., Jiang, D.-M., Wang, C.-M., Zhang, W.-G.: Effect of ba doping on magnetic and dielectric properties of nanocrystalline $BiFeO_3$ at room temperature, *J. Alloy. Compd.*, **507**, 29 – 32, (2010).

18 Das, R., Mandal, K.: Effect of barium substitution on ferroelectric and magnetic properties of bismuth ferrite, *Magnetics, IEEE Transactions on*, **47**, 4054 – 4057, (2011).

19 Luo, M., Zhou, P., Liu, Y., Wang, X., Xie, J.: Influence of Y-doping on structure, microwave dielectric and magnetic behaviors in $BiFeO_3$, *Physica B*, **450**, 1 – 6, (2014).

20 Huang, F., Lu, X., Lin, W., Wu, X., Kan, Y., Zhu, J.: Effect of nd dopant on magnetic and electric properties of $BiFeO_3$ thin films prepared by metal organic deposition method, *Appl. Phys. Lett.*, **89**, 242914, (2006).

21 Kim, J.S., Cheon, C.I., Lee, C.H., Jang, P.W.: Weak ferromagnetism in the ferroelectric BiFeO3-$ReFeO_3$-$BaTiO_3$ solid solutions (Re= dy, La), *J. Appl. Phys.*, **96**, 468 – 474, (2004).

22 Murashov, V., Rakov, D., Ionov, V., Dubenko, I., Titov, Y., Gorelik, V.: Magnetoelectric (Bi, Ln) $FeO_3$ compounds: crystal growth, structure and properties, *Ferroelectrics*, **162**, 11 – 21, (1994).

23 Uchida, H., Ueno, R., Funakubo, H., Koda, S.: Crystal structure and ferroelectric properties of rare-earth substituted $BiFeO_3$ thin films, *J. Appl. Phys.*, **100**, 4106, (2006).

24 Das, S., Bhattacharya, P., Choudhary, R., Katiyar, R.: Effect of la substitution on structural and electrical properties of $BiFeO_3$ thin film, *J. Appl. Phys.*, **99**, 6107, (2006).

25 Yuan, G., Or, S.W., Chan, H.L.W.: Structural transformation and ferroelectric-paraelectric phase transition in $Bi_{1-x}$ $La_x$ $FeO_3$ ($x$= 0 – 0.25) multiferroic ceramics, *J. Phys. D: Appl. Phys.*, **40**, 1196, (2007).

26 Gabbasova, Z., Kuz'min, M., Zvezdin, A., Dubenko, I., Murashov, V., Rakov, D., Krynetsky, I.: $Bi_{1-x}R_xFeO_3$ (R= rare earth): a family of novel magnetoelectrics, *Phys. Lett. A*, **158**, 491 – 498, (1991).

27 Bellakki, M., Manivannan, V.: Citrate-gel synthesis and characterization of yttrium-doped multiferroic $BiFeO_3$, *J. Sol-Gel Sci. Technol.*, **53**, 184 – 192, (2010).

28 Wu, Y.-J., Chen, X.-K., Zhang, J., Chen, X.-J.: Structural transition and enhanced magnetization in $Bi_{1-x}Y_xFeO_3$, *J. Magn. Magn. Mater.*, **324**, 1348 – 1352, (2012).

29 Feng, B., Xue, H., Xiong, Z.: Structure and multiferroic properties of Y-doped $BiFeO_3$ ceramics, *Chin. Sci. Bull.*, **55**, 452 – 456, (2010).

30 Chaodan, Z., Jun, Y., Duanming, Z., Bin, Y., Yunyi, W., Longhai, W., Yunbo, W., Wenli, Z.: Processing and ferroelectric properties of Ti-doped $BiFeO_3$ ceramics, *Integr. Ferroelectr.*, **94**, 31 – 36, (2007).

31 Singh, V., Sharma, S., Jha, P.K., Kumar, M., Dwivedi, R.: Effect of $Y^{3+}$ substitution on structural, electrical and optical properties of $BiFeO_3$ ceramics, *Ceram. Int.*, **40**, 1971 – 1977, (2014).

32 Shannon, R.D.: Revised effective ionic radii and systematic studies of interatomic distances in d chalcogenides, *Acta Crystall. A-Crys.*, **32**, 751 – 767, (1976).

33 Patel, P.K., Yadav, K., Singh, H., Yadav, A.: Origin of giant dielectric constant and magnetodielectric study in $Ba(Fe_{0.5}Nb_{0.5})O_3$ nanoceramics, *J. Alloy Compd.*, **591**, 224 – 229, (2014).

34 Gautam, A., Uniyal, P., Yadav, K., Rangra, V.: Dielectric and magnetic properties of $Bi_{1-x}Y_xFeO_3$ ceramics, *J. Phys. Chem. Solids*, **73**, 188 – 192, (2012).

35 Jonscher, A.K.: The 'universal' dielectric response, *Nature*, **267**, 673 – 679, (1977).

36 Dai, H., Xue, R., Chen, Z., Li, T., Chen, J., Xiang, H.: Effect of eu, ti co-doping on the structural and multiferroic properties of $BiFeO_3$ ceramics, *Ceram. Int.*, **40**, 15617 – 22, (2014).

37 Yuan, X.-P., Tang, Y.-K., Sun, Y., Xu, M.-X.: Structure and magnetic properties of $Y1-_xLuxFeO_3$ ($0 \le x \le 1$) ceramics, *J. Appl. Phys.*, **111**, 053911, (2012).

38 Shen, H., Xu, J., Wu, A., Zhao, J., Shi, M.: Magnetic and thermal properties of perovskite $YFeO_3$ single crystals, *Mater. Sci. Eng., B*, **157**, 77 – 80, (2009).

39 Luo, L., Wei, W., Yuan, X., Shen, K., Xu, M., Xu, Q.: Multiferroic properties of Y-doped $BiFeO_3$, *J. Alloy Compd.*, **540**, 36 – 38, (2012).

40 Palkar, V., John, J., Pinto, R.: Observation of saturated polarization and dielectric anomaly in magnetoelectric $BiFeO_3$ thin films, *Appl. Phys. Lett.*, **80**, 1628 – 1630, (2002).

41 Qi, X., Dho, J., Tomov, R., Blamire, M.G., MacManus-Driscoll, J.L.: Greatly reduced leakage current and conduction mechanism in aliovalent-ion-doped $BiFeO_3$, *Appl. Phys. Lett.*, **86**, 2903, (2005).